Stick-to-Sliding Transition in Contact-Resonance Atomic Force Microscopy

C. Ma,[1, 2, a)] V. Pfahl,[1] Z. Wang,[1] Y. Chen,[2] J. Chu,[2] M. K. Phani,[3, b)] A. Kumar,[3] W. Arnold,[1, 4] and K. Samwer[1]

[1)] *I. Physikalisches Institut, Georg-August-Universität Göttingen, D-37077 Göttingen, Germany*

[2)] *Department of Precision Machinery and Precision Instrumentation, University of Science and Technology of China, Hefei 230026, China*

[3)] *Metallurgy and Materials Group, Indira Gandhi Centre for Atomic Research, Kalpakkam 603102, Tamil Nadu, India*

[4)] *Department of Materials Science and Engineering, Saarland University, D-66123 Saarbrücken, Germany*

(Dated: 20 July 2018)

Contact-resonance atomic force microscopy (CR-AFM) has been used to measure the viscoelastic loss tangent of soft materials such as polymers. Usually, the damping is attributed to the dissipation in the contact volume due to internal friction and air damping of the cantilever. However, partial slip or even full sliding can exist in the contact zone under tangential loading, and thus the accompanying energy dissipation must be taken into account when measuring the damping constant Q_{loc}^{-1}. Here, the stick-to-sliding transition of the tip-sample contact in CR-AFM was studied. Amplitude drops were observed in the resonance curves caused by such stick-to-sliding transitions. The results show that the stick-to-sliding transition arises under small contact forces and large excitation amplitudes. Extra energy loss from full sliding induces large contact damping. The critical lateral displacement needed for the stick-to-sliding transition varies linearly with the contact radius.

Atomic force microscopy (AFM) was originally invented for high-resolution topography imaging. A variety of AFM modes have since then been developed in order to measure other surface or near-surface quantities. Among them, CR-AFM techniques have attracted much attention for mechanical characterization at the nanoscale.[1] In addition to the progress in elastic properties measurements[2–5] and subsurface detection of defects[6–9], CR-AFM was further developed in order to determine both the storage modulus E' and the loss modulus E''[10,11]. This was first applied to polymeric materials in order to measure the viscoelastic loss tangent.[12–14] Furthermore, local internal friction of metallic and insulating glasses[15–17] and of nanocrystalline Ni[18] was examined.

As postulated by Mindlin[19,20], micro-slip or partial slip exists in the contact area under tangential loading between contacting bodies, resulting in energy dissipation. Micro-slip was verified on the macro- and the microscale[21–24] and it has been suggested that in tip-sample contacts it contributes to damping in CR-AFM[15–17,25].

A clear understanding of the tip-sample contact mechanism under tangential loading as well as the influence of interfacial friction on CR-AFM measurements is still missing. Therefore, we studied the transition from sticking to total sliding of the tip-sample contact in CR-AFM. The conditions for the initiation of lateral sliding of the tip-sample contact pair were investigated, and the stick-to-sliding induced effects both on the cantilever response and the measured contact damping were analyzed.
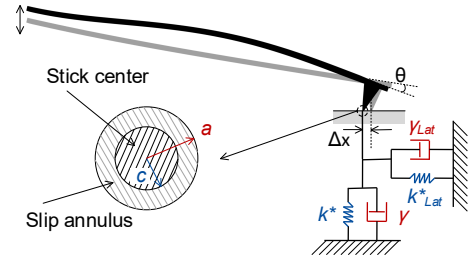
[a)] Electronic mail: chfuma@ustc.edu.cn
[b)] Present address: OP Jindal University, Raigarh 496109, Chhattisgarh, India

FIG. 1. Illustration of a vibrating AFM cantilever with the tip under viscoelastic contact, which is modeled by Kelvin-Voigt elements (k^*, γ), $(k_{Lat}^*, \gamma_{Lat})$ in the normal and lateral directions, respectively. The inset demonstrates the tip-sample contact area under tangential loading, with a stick center and a slip annulus. The cantilever is tilted by 11° due to technical reasons.

In CR-AFM, the tip-sample contact is usually modeled by Kelvin-Voigt elements (Fig. 1). Assuming small vibration amplitudes, the tip-sample contact forces are approximated by elastic and viscoelastic forces. Contact forces are represented by springs and dashpots both in the normal (k^*, γ) and the lateral $(k_{Lat}^*, \gamma_{Lat})$ directions. Models describing the cantilever dynamics without damping lead to characteristic equations between the contact stiffness and the wave number of the cantilever motion.[1,3] When taking damping into account, a complex wave vector $\eta = (\kappa_r + i\kappa_i)/L$ describing the cantilever's motion is introduced, with L the cantilever length. In this way the mode-shape of the cantilever is taken into account. The real part κ_r and the imaginary part κ_i can be determined from the measured free and contact-resonance frequencies with their quality factors (f^{FR}, Q^{FR}) and (f^{CR}, Q^{CR}) by fitting the resonance curves to Lorentzians (see also supplementary material).[12] This

yields a complex contact stiffness $k^* = k_r + i k_i$, where k_r is the real part of the contact stiffness and $k_i = \omega\gamma$ is the imaginary part, with ω the angular frequency. The local contact-damping factor is then given by $Q_{loc}^{-1} = \tan\delta = E''/E' = \omega\gamma/k_r = k_i/k_r$. Here, $k_r = 2aE'$ and $k_i = 2aE''$ where a is the tip-sample contact radius.

As illustrated in Fig. 1, the flexural vibration of the cantilever in contact induces a periodical deflection with angular amplitude θ at the tip position, leading to a periodical lateral displacement of the tip apex. If the tip is free, this displacement is $\Delta x = \tan\theta \cdot h$, with h the tip height. When the tip is in contact and not sliding, a tangential force develops. According to Mindlin's theory[19–22,26], increasing tangential forces result in progressive micro-slipping contacts. In the contact area with radius a, tip-sample slip first arises in an annulus at the periphery of the contact as partial slip, whereas in the circular center of radius c the tip still sticks to the surface. With increasing lateral displacement Δx, the slip area increases and the stick center decreases, until a critical displacement D is reached where the stick center vanishes, initiating total sliding. For a constant normal load of F_N, the lateral force is $F_L = F_T + F_F$ during this process. Here, F_T is the shear force in the stick center, $F_F = \mu F_N$ is the friction force in the slip annulus, and μ is the friction coefficient. Total sliding sets in when $F_L = F_F$.

In order to study the stick-to-sliding transition and its influence on the CR-AFM measurements, CR spectra were acquired under various applied tip loads and excitation amplitudes. The experiments were performed with a Dimension Icon, Bruker Nano AFM. Cantilever oscillations were either induced by a transducer beneath the sample (atomic force acoustic microscopy, AFAM mode) or via the piezo-shaker under the cantilever chip (ultrasonic atomic force microscopy, UAFM mode). All measurements were carried out with the same silicon AFM probe (MPP-21100-10, Bruker Nano), prior to which the fresh tip was scanned in order to reach a steady wear state. The static inverse optical lever sensitivity ($InvOLS$) was determined to be about 92 nm/V. The cantilever's spring constant was measured to be 5.8 N/m using the thermal method. The free resonance of the first eigenmode in air was $f^{FR} = 85.4$ kHz and its Q-value $Q^{FR} = 131$. The samples used were a silicon wafer and a 40 nm thin film of $La_{0.6}Sr_{0.4}MnO_3$ (LSMO) deposited on a single-crystal $SrTiO_3$ (111) substrate[17]. The measured root mean square roughness (Rq) of the samples in 1.5×1.5 μm^2 test areas were 0.93 nm for the Si sample and 1.09 nm for the LSMO sample. All measurements were conducted in humidity controlled air ($\approx 33\%$) at 290 K.

Fig. 2 shows the contact-resonance curves for the first cantilever mode on the silicon sample obtained with the AFAM technique. Tests were carried out with eleven different excitation amplitudes from 0.1 V to 3.0 V, each with thirteen different tip loads from 31 nN to 325 nN. All tests were repeated five times for each case under the same excitation amplitude and tip load. The pull-off forces, around 84 nN for the silicon sample and 35 nN for the LSMO sample, were included in the total tip loads for all measurements. To calibrate the amplitude, an FEA model of the cantilever dynamics was used.[27] For simplicity, a single value for the calibration factor ($InvOLS^{CR}$) of 9.9 nm/V determined for a CR frequency of 400 kHz, was used to calibrate the normal amplitudes in Figs. 2 and 4(b) for all frequencies. This entails a maximum error of 7%. Moreover, the deflection angle θ, and thus the lateral displacement Δx can also be calibrated from the model. Other parameters used in the calibration model are listed in reference [38].
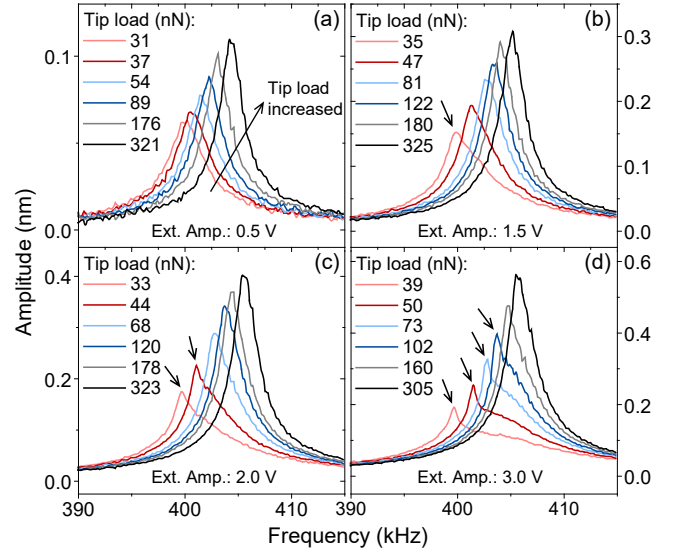

FIG. 2. AFAM amplitude spectra of the first contact-resonance on a silicon wafer under different applied tip loads and excitation amplitudes: (a) - (d): excitation amplitudes of 0.5, 1.5, 2.0, and 3.0 V, respectively. For clarity, only a few typical spectra are shown.

The amplitudes of the contact-resonance curves depend on the excitation amplitudes and on the static loads (Fig. 2). They increase approximately linearly with the excitation amplitude for all static loads. Furthermore, larger static loads increase the contact area leading to larger contact stiffness and hence to higher CR frequencies.[1] In addition, the amplitude becomes larger because an increase in contact stiffness entails a larger Q-value for the same damping as noticed by various groups and worked out in detail earlier[11].

With increasing excitation, nonlinear behavior gradually arises in the cantilever frequency response under small tip load. Some of the distortions are highlighted by arrows in Figs. 2(b)-(d), marked by sudden amplitude drops. When applying higher tip loads, larger excitation amplitudes are needed to reach a critical value again. Moreover, for the same excitation, by increasing the tip load, the nonlinear behavior gradually disappears and the spectra return to Lorentzian shapes. This is a strong hint that the nonlinearity originates in the boundary

of the tip-sample contact. Strictly speaking, the nonlinear behavior precludes the fit of the resonance curves with Lorentzians. However, as can be seen experimentally, the overall shape of the resonance curve remains close to Lorentzian and therefore we continue to use the procedure of Yuya et al[11] to evaluate the local damping. Further details are discussed in the supplementary material.

The resonance shapes described here are different from the frequency response due to a softening nonlinearity caused by tip-sample adhesion[28] (see also supplementary material). Nonlinear frequency response curves have also been used to reconstruct force-distance curves[29]. To this end, large normal amplitudes were applied in order to sweep the full force-distance curve at various static loads using the second cantilever mode. Finally, in torsional contact-resonance experiments plateaus in the frequency response have been observed when exceeding critical amplitudes[30].

To interpret the data, we suggest a stick-to-sliding transition for the tip-sample contact facilitated by the small lift-off due to sonolubrication[27]. A typical contact-resonance showing nonlinear behavior taken on the silicon sample is shown in the inset of Fig. 3 which was taken by sweeping from low to high frequency. When the frequency is far from the CR, the cantilever amplitude and also the lateral displacement amplitude of the tip are small, resulting in a lateral contact force smaller than the tip sticking-force. Then, when approaching the CR frequency, the cantilever amplitude and also the tip lateral displacement get larger, leading to a micro-slip contact between the tip and the sample with increased shear force in the stick center and an expanding slip annulus starting from the contact periphery. Finally, at a critical point, the relative lateral displacement becomes so large that the shear force in the stick center exceeds the static friction force and the slip annulus expands to the entire contact area, resulting in a sudden transition from stick to total sliding of the tip-sample contact. Correspondingly, the sudden change of the contact condition and also the reduction of the lateral force to a kinetic friction force induce a drop of the cantilever amplitude. This is similar to the transition from static friction to kinetic friction[31]. For further details, see supplementary materials.

The amplitude drops in the CR spectra can be used as indicators of the initiation of total sliding. By manually extracting the critical cantilever amplitudes where the amplitude drops occur and with calibration of the lateral displacements, we determined the critical lateral displacements D to initiate total sliding on the silicon sample (AFAM) and on the LSMO sample (UAFM) under various tip loads F_N. The results show power-law relationships $D \sim C(F_N - F_{offset})^n$ for both samples where C is a constant. Best fits gave $n = 0.486 \pm 0.030$ for the LSMO sample and 0.391 ± 0.093 for the silicon sample. The offset forces F_{offset} used in the fits[32] are close to 23 nN for both samples. They indicate lower
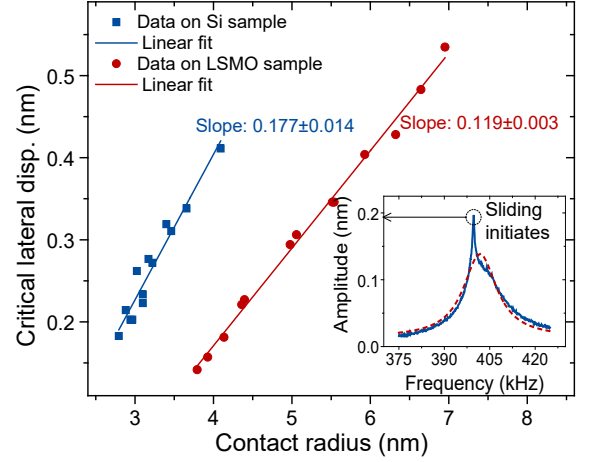

FIG. 3. Critical lateral displacement amplitudes D of the tip to initiate total sliding as a function of contact radius a both on the silicon sample and the LSMO sample. The solid lines represent linear fits. Inset: Typical nonlinear behavior of a contact-resonance on the silicon sample displaying an amplitude drop; the dashed curve represents a Lorentzian fit of the resonance curve.

adhesion forces compared to the pull-off forces. This is most likely due to the fact that the contact is neither spherical nor flat.

We relate the critical displacements D with the contact radius a. The latter is calculated from the static load F_N with $a = (3F_N R/4E^*)^{1/3}$ by considering a Derjaguin-Muller-Toporov (DMT) contact[32], where R is the tip radius (≈ 80 nm as measured by SEM) and E^* is the reduced Young's modulus. Here, $E^* = 91$ GPa for Si and $E^* = 42$ GPa for LSMO using $1/E^* = (1-\nu_t^2)/E_t + (1-\nu_s^2)/E_s$ where (E_t, ν_t), (E_s, ν_s) are respectively the Young's modulus and the Poisson's ratio of the tip and the sample, which are (169 GPa, 0.27) for the tip and the Si sample, and (50 GPa, 0.3) for the LSMO sample[27]. A nearly linear relation can be found between D and the contact radius a for both materials (Fig. 3). The slopes are 0.177 ± 0.014 for the silicon sample and 0.119 ± 0.003 for the LSMO sample. The finite intercepts in the experimental data are caused by adhesion. Considering the friction force $F_F = \tau A = \tau \pi a^2$ for a single asperity contact, the linear relationship $D \sim a$ agrees with the Mindlin theory[20,23] where $D = 3F_F/16aG^* = (3\pi/16)(\tau/G^*)a$. Here, τ is the shear strength, A is the contact area, and G^* is the reduced shear modulus as $1/G^* = (2-\nu_t)/G_t + (2-\nu_s)/G_s$ where G_t and G_s are respectively the shear modulus of the tip and the sample. From this relation, one obtains $\tau/G^* = 0.300$ and 0.202 for Si and LSMO, respectively. Taking $G^*_{Si-Si} = 18.9$ GPa and $G^*_{Si-LSMO} = 8.7$ GPa[17], one obtains $\tau_{Si} \approx 5.7$ GPa for Si and $\tau_{LSMO} \approx 1.7$ GPa for LSMO. These values are smaller than that obtained for small-scale objects[33,34] of the same materials supporting the view that single asperity contacts can be regarded as cracks in an infinite medium[35].
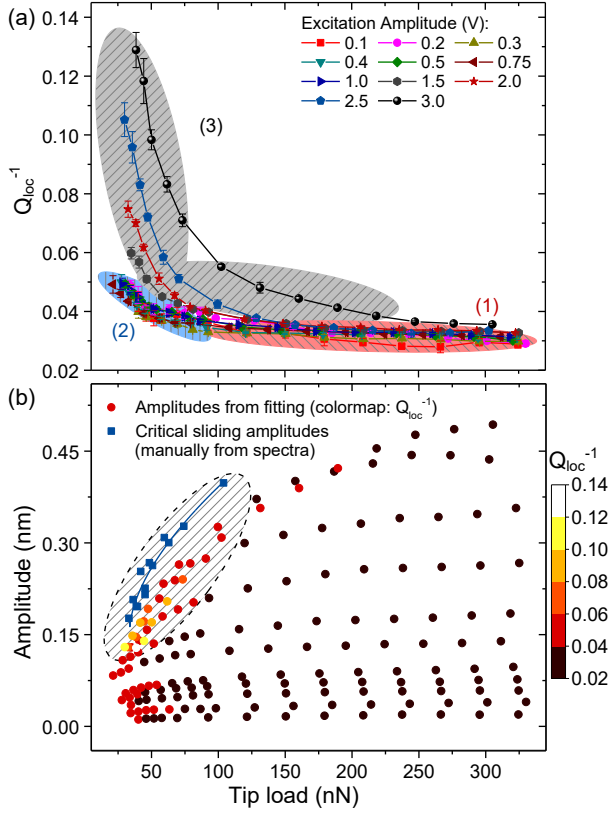
FIG. 4. (a) Q_{loc}^{-1} mean values on Si with standard deviations in five measurements under different tip loads and excitation amplitudes; (b) All fitted cantilever amplitude data-sets for Si under different tip loads, with the Q_{loc}^{-1} mean values shown in a colored map. Data in solid squares are the critical cantilever amplitudes extracted manually from the spectra exhibiting a nonlinear amplitude drop.

Additional energy dissipation is expected during the sudden stick-to-sliding transition and the subsequent sliding friction. This can be unambiguously observed from the widened and flattened spectra where full sliding happens (Fig. 2). We investigated the contribution of the stick-to-sliding transition to the damping of CR more quantitatively. Fig. 4(a) shows the averaged Q_{loc}^{-1} for the silicon sample with standard deviation error bars for five measurements. For all excitations, Q_{loc}^{-1} decreases gradually with increasing applied tip load until it stabilizes at large contact forces. However, for the larger excitation amplitudes of 1.5, 2.0, 2.5 and 3.0 V, differences can still be seen. Q_{loc}^{-1} is increased under small loads, e. g. those smaller than 200 nN for the 3.0 V excitation amplitude case, compared with smaller excitations, indicating the presence of tip sliding.

The Q_{loc}^{-1} data can be divided into three regions depending on the tip load and the excitation amplitude, as shown in Fig. 4(a). In region (1) with a large static load, Q_{loc}^{-1} becomes stable with internal friction in the contact volume becoming noticeable. A small amount of energy dissipation due to micro-slip may still exist in this region. For larger contact forces, additional dissipation may arise from material abrasion or plastic deformation. In region (2), near the attractive regime, adhesion dissipation plays a large role as studied earlier[28,36] which also results in local damping. For small loads but large excitation amplitudes in region (3), total sliding sets in, dominating Q_{loc}^{-1}.

Furthermore, we plotted in Fig. 4(b) all cantilever amplitude data under different loads from Lorentzian fits, with the corresponding Q_{loc}^{-1} values indicated by a colored bar. The region shown in the dashed area with significantly increased Q_{loc}^{-1} values determines under what conditions stick-to-sliding occurs. For comparison, we also plotted the critical cantilever amplitudes from spectra showing nonlinear amplitude behavior (Fig. 4(b)). The sliding region determined by Q_{loc}^{-1} values agrees well with the sliding condition defined by the amplitude drops.

We conclude that the resulting Q_{loc}^{-1} in CR-AFM is determined also by several other contributions in the tip-sample contact volume besides internal friction of the material: (i) adhesion dissipation; (ii) friction by partial micro-slip; (iii) frictional dissipation from stick-to-sliding events; and (iv) air damping[15,37]. With increasing tip load, the role of adhesion diminishes and micro-slips and stick-to-sliding events are suppressed. This leads to a gradual reduction of Q_{loc}^{-1}, implies an accurate measure of the internal friction under large elastic loads. For materials with small internal friction, air damping becomes the dominant contribution to Q_{loc}^{-1} at high enough static loads and thus determines the lower limit of Q_{loc}^{-1} measurements using CR-AFM in air which is of the order of 10^{-3} to 10^{-2}. However, relative damping measurements where one takes a reference point on the sample itself or on a calibration material, remain a possibility to measure small changes of Q_{loc}^{-1}.[10–12,15] Finally, our data further support that Mindlin's theory for macroscopic contacts also applies to AFM tip-sample contacts[23,25,30].

See supplementary material for our discussions on the resonance shape under a stick-to-sliding process and the energy dissipation by micro-slip.

[1]U. Rabe, M. Kopycinska-Müller, and S. Hirsekorn, in *Acoustic Scanning Probe Microscopy*, Eds. F. Marinello, D. Passeri, and E. Savio (Springer Berlin Heidelberg, 2013), pp. 123-153.

[2]D. C. Hurley, M. Kopycinska-Müller, A. B. Kos, and R. H. Geiss, Meas. Sci. Technol. **16**, 2167 (2005).

[3]D. C. Hurley and J. A. Turner, J. Appl. Phys., **102**, 033509 (2007).

[4]H. Wagner, D. Bedorf, S. Küchemann, M. Schwabe, B. Zhang, W. Arnold, and K. Samwer, Nat. Mater., **10**, 439 (2011).

[5]M. R. Rosenberger, S. Chen, C. B. Prater, and W. P. King, Nanotechnology, **28**, 044003 (2017).

[6]T. Tsuji and K. Yamanaka, Nanotechnology, **12**, 301 (2001).

[7]D. C. Hurley, M. Kopycinska-Müller, E. D. Langlois, A. B. Kos, and N. Barbosa III, Appl. Phys. Lett., **89**, 021911 (2006).

[8]A. Yao, K. Kobayashi, S. Nosaka, K. Kimura, and H. Yamada, Sci. Rep., **7**, 42718 (2017).

[9]C. Ma, Y. Chen, W. Arnold, and J. Chu, J. Appl. Phys., **121**, 154301 (2017).

[10]P. A. Yuya, D. C. Hurley, and J. A. Turner, J. Appl. Phys., **104**, 074916 (2008).

[11]P. A. Yuya, D. C. Hurley, and J. A. Turner, J. Appl. Phys., **109**, 113528 (2011).

[12]J. P. Killgore, D. G. Yablon, A. H. Tsou, A. Gannepalli, P. A. Yuya, J. A. Turner, R. Proksch, and D. C. Hurley, Langmuir, **27**, 13983 (2011).

[13]D. C. Hurley, S. E. Campbell, J. P. Killgore, L. M. Cox, and Y. Ding, Macromolecules, **46**, 9396 (2013).

[14]A. B. Churnside, R. C. Tung, and J. P. Killgore, Langmuir, **31**, 11143 (2015).

[15]H. Wagner, M. Büchsenschütz-Göbeler, Y. Luo, A. Kumar, Arnold, W., and K. Samwer, J. Appl. Phys., **115**, 134307 (2014).

[16]M. K. Phani, A. Kumar, T. Jayakumar, W. Arnold, and K. Samwer, Beilstein J. Nanotech., **6**, 767 (2015).

[17]V. Pfahl, M. K. Phani, M. Büchsenschütz-Göbeler, A. Kumar, V. Moshnyaga, W. Arnold, and K. Samwer, Appl. Phys. Lett., **110**, 053102 (2017).

[18]A. Caron and W. Arnold, Acta Mater. **57**, 4353 (2009).

[19]R. D. Mindlin, J. Appl. Mech., **16**, 259 (1949).

[20]R. D. Mindlin and H. Deresiewicz, J. Appl. Mech., **20**, 327 (1953).

[21]K. L. Johnson, J. Mech. Eng. Sci., **3**, 362 (1961).

[22]M. Eguchi, T. Shibamiya, and T. Yamamoto, Tribol. Int., **42**, 1781 (2009).

[23]P. E. Mazeran and M. Beyaoui, Tribol. Lett., **30**, 1 (2008).

[24]M. Paggi, R. Pohrt, and V. L. Popov, Sci. Rep., **4**, 5178 (2014).

[25]A. Caron, W. Arnold, and H. J. Fecht, Jpn. J. Appl. Phys., **49**, 120204 (2010).

[26]K. L. Johnson, Proc. R. Soc. Lond. A, **230**, 531 (1955).

[27]V. Pfahl, C. Ma, W. Arnold, and K. Samwer, J. Appl. Phys., **123**, 035301 (2018).

[28]M. Muraoka and W. Arnold, JSME Int. J. A-Solid M., **44**, 396 (2001).

[29]D. Rupp, U. Rabe, S. Hirsekorn, and W. Arnold, J. Phys. D: Appl. Phys., **40**, 7136 (2007).

[30]M. Reinstädtler, U. Rabe, V. Scherer, U. Hartmann, A. Goldade, B. Bhushan, and W. Arnold, Appl. Phys. Lett., **82**, 2604 (2003).

[31]R. W. Carpick, D. F. Ogletree, and M. Salmeron, Appl. Phys. Lett., **70**, 1548 (1997).

[32]E. Gnecco, R. Bennewitz, O. Pfeiffer, A. Socoliuc, and E. Meyer, in *Springer Handbook of Nanotechnology*, Ed. B. Bhushan (Springer Berlin Heidelberg, 2004), pp. 646-649.

[33]B. Bhushan, in *Springer Handbook of Nanotechnology*, Ed. B. Bhushan (Springer Berlin Heidelberg, 2004), pp. 763-785.

[34]S. Jiang, X. Ma, G. Tang, G. Wang, Z. Wang, and Z. Zhou, Thin Solid Films, **519**, 4880 (2011).

[35]R. W. Carpick, E. E. Flater, K. Sridharan, D. F. Ogletree, and M. Salmeron, JOM, **56**, 48 (2004), and reference contained therein.

[36]R. Szoszkiewicz, A. J. Kulik, and G. Gremaud, J. Chem. Phys., **122**, 134706 (2005).

[37]H. Hosaka, K. Itao, and S. Kuroda, Sensor. Actuat. A-Phys, **49**, 87 (1995).

[38]Parameters used in the FEA calibration model are: cantilever length $L = 225$ μm, width $w = 43$ μm, thickness $t = 2.91$ μm, cantilever tilt $\alpha_0 = 11°$, tip height $h = 16$ μm, tip position $L_1 = 215$ μm, the ratio λ between the normal and lateral contact stiffness $\lambda = k^*_{Lat}/k^* = 0.85$. Same values for L, L_1, α_0, h, λ are used in the analytical model of calculating Q^{-1}_{loc} values from the CR-data as in the FEA model.